Published online 20 March 2023

Nucleic Acids Research, 2023, Vol. 51, No. 8 **3855–3868**
https://doi.org/10.1093/nar/gkad154

SPIDR is required for homologous recombination during mammalian meiosis

Tao Huang[1,4,5,6,9,†], Xinyue Wu[1,4,5,6,†], Shiyu Wang[1,4,5,6], Ziyou Bao[1,4,5,6], Yanling Wan[1,4,5,6], Ziqi Wang[1,4,5,6], Mengjing Li[1,4,5,6], Xiaochen Yu[1,4,5,6], Yue Lv[2,9], Zhaojian Liu[7], Xiangfeng Chen[8], Wai-Yee Chan[1,4,5,6,9], Fei Gao[1,4,5,6,9], Gang Lu[1,4,5,6,9,*], Zi-Jiang Chen[1,2,3,4,5,6,8,9,*] and Hongbin Liu[1,3,4,5,6,9,*]

[1]Center for Reproductive Medicine, Shandong University, Jinan, Shandong 250012, China, [2]Shandong Key Laboratory of Reproductive Medicine, Shandong Provincial Hospital Affiliated to Shandong First Medical University, Jinan, Shandong, China, [3]Research Unit of Gametogenesis and Health of ART-Offspring, Chinese Academy of Medical Sciences, China, [4]Key Laboratory of Reproductive Endocrinology of Ministry of Education, Shandong University, Jinan, Shandong 250012, China, [5]Shandong Provincial Clinical Medicine Research Center for Reproductive Health, Jinan, Shandong 250012, China, [6]Shandong Technology Innovation Center for Reproductive Health, Jinan, Shandong 250012, China, [7]Advanced Medical Research Institute, Shandong University, Jinan, China, [8]Shanghai Key Laboratory for Assisted Reproduction and Reproductive Genetics, Shanghai 200135, China and [9]CUHK-SDU Joint Laboratory on Reproductive Genetics, School of Biomedical Sciences, the Chinese University of Hong Kong, Hong Kong, China

Received December 11, 2022; Revised February 17, 2023; Editorial Decision February 19, 2023; Accepted February 21, 2023

ABSTRACT

Meiotic recombinases RAD51 and DMC1 mediate strand exchange in the repair of DNA double-strand breaks (DSBs) by homologous recombination. This is a landmark event of meiosis that ensures genetic diversity in sexually reproducing organisms. However, the regulatory mechanism of DMC1/RAD51-ssDNA nucleoprotein filaments during homologous recombination in mammals has remained largely elusive. Here, we show that SPIDR (scaffold protein involved in DNA repair) regulates the assembly or stability of RAD51/DMC1 on ssDNA. Knockout of *Spidr* in male mice causes complete meiotic arrest, accompanied by defects in synapsis and crossover formation, which leads to male infertility. In females, loss of *Spidr* leads to subfertility; some *Spidr*$^{-/-}$ oocytes are able to complete meiosis. Notably, fertility is rescued partially by ablation of the DNA damage checkpoint kinase CHK2 in *Spidr*$^{-/-}$ females but not in males. Thus, our study identifies SPIDR as an essential meiotic recombination factor in homologous recombination in mammals.

INTRODUCTION

Meiosis is the process of cell division of diploid progenitors into haploid gametes in sexually reproducing organisms. Erroneous meiosis generates aberrant gamete which can cause fertility defects, or even infertility (1). During meiosis, homologous chromosomes pair, synapse and undergo homologous recombination (HR) in order to ensure proper segregation (2). Recombination is initiated by programmed DNA double-strand breaks (DSBs) which are generated by SPO11 (3). SPO11 is subsequently removed together with an oligonucleotide chain under the action of endonuclease MRE11, after which DSB ends are further resected by the exonuclease to generate single strand 3' overhangs (4,5). This single stranded DNA (ssDNA) is protected by replication protein homologs (RPAs). Subsequently, the RecA-like proteins RAD51 and its meiosis-specific homolog DMC1 are recruited by BRCA2, which will replace RPA and mediate strand-invasion and promote the formation of displacement loop (D-loop) (6,7). After D-loop formation, meiotic DSBs are repaired by the synthesis-dependent strand annealing (SDSA) pathway or by the double Holiday-Junction (dHJ) pathway (8,9). In the dHJ pathway, the extended D-loop is captured by another terminal single chain of DSB, and the new chain is synthesized with a homologous chromosome as a template. Finally, it forms an intermediate called dHJ, a CO-specific form of recombination

*To whom correspondence should be addressed. Tel: +86 531 85651190; Email: hongbin_sduivf@aliyun.com
Correspondence may also be addressed to Zi-Jiang Chen. Email: chenzijiang@hotmail.com
Correspondence may also be addressed to Gang Lu. Email: lugang@cuhk.edu.hk
†The authors wish it to be known that, in their opinion, the first two authors should be regarded as Joint First Authors.

intermediate specifically resolved to COs by the MLH1–MLH3 complex (10,11).

The meiotic recombinases RAD51 and DMC1 mediate homologous recombination by promoting the nucleoprotein filament to search and invade its homologous chromosome. The mechanisms regulating DMC1/RAD51-ssDNA nucleoprotein filaments remain to be clarified. SPIDR is considered as a highly conserved protein with no identified motifs (Supplementary Figure S1E), and was initially proposed to function as a scaffolding protein. Accordingly, this protein would promote the assembly of subnuclear RAD51 foci and regulate the ratio of crossover-to-non-crossover recombinants via BLM helicase, in order to promote HR efficiency (12). SPIDR was shown to function as an efficient HR factor acting through several HR-related molecules such as FIGNL1 (fidgetin-like 1), SWSAP1, and SWS1 in somatic cells (13–16). The SWS1–SWSAP1 complex is a recently identified complex that functions in promoting the stable assembly of both RAD51 and DMC1 nucleoprotein filaments during meiosis (17). SPIDR is a subunit of the SWS1–SWSAP1–SPIDR complex regulating interhomolog homologous recombination (IH-HR) (18). However, its role in homologous recombination during meiosis is not well understood.

In this study, we knocked out *Spidr* in mice, seeking to characterize its function(s) in meiotic recombination. We found that during meiosis SPIDR recruits RAD51 and DMC1 for the formation or stabilization of nucleoprotein filaments. Deletion of *Spidr* completely blocked the progression of meiosis, and this was accompanied by defects in DSB repair and synapsis, which rendered failure in male spermatogenesis. Primary ovarian insufficiency (POI) is a subclass of ovarian dysfunction in which an unknown mechanism leads to premature exhaustion of the primordial follicle pool (PFP) (19). We found that *Spidr*-deficient females showed defects of meiosis and decrease in fertility similar to human POI—the phenotype resulting from severe exhaustion of PFP (19–23). Remarkably, *Spidr*-deficient fertility could be restored by the ablation of the DNA damage checkpoint kinase CHK2 in females, but not in males.

MATERIALS AND METHODS

Generation of *spidr* and *chk2* knockout mice

The mouse *Spidr* gene is located on chromosome 16. *Spidr* knockout mice in a B6D2F2 genetic background were constructed by deleting genomic DNA fragments covering exon 2 to exon 3 using CRISPR/Cas9 system entrusted to the Institute of Zoology, Chinese Academy of Sciences.

Chk2 knockout mice in a C57BL/6JGpt genetic background were constructed by deleting genomic DNA fragments covering exon 3 to exon 6 using CRISPR/Cas9 system. The founders were genotyped by polymerase chain reaction (PCR), followed by DNA sequencing analysis.

Mouse care

The care and use of mice in this study were carried out according to the protocol approved by the animal management center of Shandong University. Mice were raised in the animal management center of Shandong University in accordance with the guidelines of the animal ethics committee and the Animal Care and Use Committee of Shandong University. All experimental protocols were approved by the Ethics Committee of Shandong University.

Genotyping

Genotyping was performed by PCR amplification of genomic DNA extracted from mouse tails. The PCR primers for *Spidr*-deficient genotyping are as follows: the mutant alleles were 5′- GGA ACC AGA GGC CAG ATA GCC CAG AGA C-3′ and 5′-CCA CTT GGA GTT GAG CTT TGT GCA AGG TGA CAA AT-3′, yielding a 653–base pair (bp) fragment; the wild-type alleles were 5′-GGA ACC AGA GGC CAG ATA GCC CAG AGA C-3′ and 5′-CCA CTT GGA GTT GAG CTT TGT GCA AGG TGA CAA AT-3′, yielding a 657–base pair (bp) fragment.

The PCR primers for *Chk2*-deficient genotyping are as follows: the mutant alleles were 5′- GGA CTT TTG GGA TGG CAT TTG AA-3′ and 5′-GCA TAG CAC TTA GGT CAG GAT TAA ACC-3′, yielding a 287–base pair (bp) fragment; the wild-type alleles were 5′-GCC CTT GAT TGT CTT CTT ACT GCT GT-3′ and 5′-TCC GAG GAG AGA AGC AAC CGTTA-3′, yielding a 316-base pair (bp) fragment.

Tissue collection and histological analysis

Immediately after euthanasia, the testes and ovaries were dissected and fixed in 4% paraformaldehyde (p1110, Solarbio, Beijing, China) for 24 h. After dehydration, they were embedded in paraffin. Prepare sections (5 μm) on glass slides. After dewaxing and hydration, the slides were stained with hematoxylin and eosin, then dehydrated and mounted for histological analysis.

Fertility test

Males: Each male mouse (8–12 weeks, $n = 3$) was caged with two wild-type C57BL/6 females (4–6 weeks), that were checked for vaginal plugs every morning. Once a vaginal plug was identified (day 1 postcoitus), the male was allowed to rest for 2 days, after which another female was placed in the cage for another round of mating. The plugged female was separated and singly caged, and the pregnancy was recorded. If a female did not generate any pups by day 22 postcoitus, it was deemed as not pregnant and euthanized to confirm result. The fertility test lasted for 2 months.

Females: Every three female mice (5 weeks) were caged with one wild-type C57BL/6 male mouse having normal fertility. The number of pups was recorded for each pregnancy. The cumulative pups of each female were calculated. The fertility test lasted for 6 months.

Immunocytology and antibodies

Spermatocyte and oocyte chromosome spreading was performed as previously described (24). Produced antibody used for western blotting: Mouse anti-SPIDR polyclonal antibody was prepared against mouse SPIDR protein by Dai-an Biological Technology Incorporation (Wuhan,

China). Primary antibodies used for immunofluorescence were as following: rabbit anti-SYCP1 (1:500 dilution; Abcam #ab15090), mouse anti-SYCP3 (1:500 dilution; Abcam #ab97672), rabbit anti-RPA2 (1:200 dilution; Abcam #ab76420), rabbit anti-RAD51 (1:200 dilution; Thermo Fisher Scientific #PA5-27195), rabbit anti-DMC1 (1:200 dilution; homemade); mouse anti-γH2AX (pSer139) (1:1000 dilution; Millipore #05–636), mouse anti-MLH1 (1:100 dilution; BD Bios*ciences* #550838), rabbit anti-BLM (1:200 dilution; Invitrogen #PA5-27384), rabbit anti-MSH4(1:200 dilution; Abcam #ab58666); rat anti-HEI10 (1:100 dilution; homemade); Rabbit anti-MSY2(1:200 dilution; Abcam #ab33164). Primary antibodies were detected with Alexa Fluor 488- or 594-conjugated secondary antibodies (1:500 dilution; Abcam #ab150080, #ab150077, #ab150113 and #ab150116) for 1 h at room temperature. The slides were mounted using Mounting Medium with DAPI (Abcam #ab104139).

Western blotting

Testes were separated from the mice, washed with PBS. According to the invent Kit (Invent #SD-001/SN-002), total protein was extracted. After denaturation, equal amounts of protein were electrophoresed on 10% SDS polyacrylamide gels, and the bands were transferred to polyvinylidene fluoride membranes (Millipore, USA). Immunoreactive bands were detected and analyzed with a Bio-Rad ChemiDoc MP imaging System and Image Lab Software (Bio-Rad, USA). The primary antibodies for immunoblotting included anti-Actin (1:5000 dilution; Cell Signaling Technology, #66009-1-Ig) and anti-SPIDR (1:1000 dilution; produced as described above).

RT-PCR

Total RNA was extracted from the testicular sorting cells of wild-type mice. cDNA was synthesized by PrimeScript RT reagent Kit with gDNA Eraser (Takara). Qualitative PCR was performed using TB Green Premix Ex Taq (Takara) and specific forward and reverse primers as follows: *Actin* primer pair, 5′-GGC TGT ATT CCC CTC CAT CG-3′ (forward) and 5′-CCA GTT GGT AAC AAT GCC ATG T-3′ (reverse). *Spidr* primer pair, 5′-CA G CAG TTG AGA CGG GGA A-3′ and 5’-ATC CTT CTC CAC ACT TGA GCC-3′ (forward). All reverse transcription PCR reactions were performed with an initial denaturation at 95°C for 10 min followed by 25 cycles of denaturation at 95°C for 30 s, annealing at 60°C for 30 s, extension at 72°C for 30 s, and a final extension at 72°C for 5 min.

Plasmids and CO-IP

Full-length cDNAs encoding *Spidr, Rad51* and *Dmc1* were amplified by RT-PCR from murine testis RNA. Full-length cDNAs were cloned into the pcDNA3.1 mammalian expression vectors. HEK 293T was maintained in DMEM supplemented with 10% FBS and 1% penicillin and streptomycin in a 37°C incubator with 5% CO2. Cell transfection was performed using lipofectamine 3000 (Invitrogen), following the manufacturer’s protocol. The same amount of antibody and IgG were added into the cell extract and the mixture was incubated at 4°C overnight. After incubation, immunocomplexes were isolated by adsorption to protein A/G Sepharose beads for 2 h. The beads were added loading buffer in proportion, boiled at 95°C, and loaded onto 10% Tris-Glycine Mini Gels (Invitrogen).

Yeast two hybrid assay

Mouse *Spidr* cDNA was subcloned into pGBKT7 vector as bait. Mouse *Rad51*, *Dmc1* cDNA were separately subcloned into pGADT7 vector as prey. The bait and prey plasmids were co-transformed into a Y2H gold strain and the interaction was tested on DDO/TDO/3AT/QDO medium.

Oocyte *in vitro* maturation and *in situ* chromosome counting

Oocytes were isolated from female mice at the age of 3–4 weeks. To get fully grown GV-stage oocytes, mice were super-stimulated with 5 IU pregnant mare’s serum gonadotropin (PMSG) injection. After 48 h of PMSG injection, cumulus oocyte complexes were obtained by manually rupturing the ovarian follicle structure. The oocytes were cultured in the small drops of M16 (M7292; Sigma-Aldrich) and maintained in 5% CO_2 at 37°C for 8 and 16 h until they arrived to metaphase I and metaphase II. Oocytes were exposed to Tyrode’s buffer (pH 2.5) for 30 s at 37°C to remove zona pellucida and fixed in a drop of 1% paraformaldehyde with 0.15% Triton X-100 on a glass slide. After air drying, oocytes were stained with the Topoisomerase II antibody (1:400 dilution; Abcam #ab109524) to detect chromosomes.

Immunohistochemistry

The ovaries of E13.5, E15.5, PD1, PD8 and PD15 were immunohistochemical. Immunohistochemistry and quantification of ovarian follicles were performed as previously (24).

Imaging

Chromosome spreads were imaged by confocal microscopy (Andor Dragonfly spinning disc confocal microscope driven by Fusion Software) and Imaris software was used to process the images. Histological samples were taken by fluorescence microscope (bx52, Olympus), Photoshop (Adobe), and ImageJ (v.1.52a) were used for image processing to count foci and quantify fluorescence.

Statistical analysis

Data were analyzed by GraphPad prism 8.0.1. Data difference between the two groups was tested by unpaired, two-tailed Student *t*-test. The error bars stand for means ± SD. The sample size has been described in the Figure legend. The significance threshold was set at P value <0.05.

RESULTS

The *spidr* knockout mice phenotype is sexually dimorphic

To investigate the role of *Spidr* in mice, we disrupted *Spidr* in B6D2F2 mice by deleting exons 2–3 using CRISPR-Cas9

genome editing; this was performed in order to generate *Spidr*-deficient (*Spidr*$^{-/-}$) mice (Figure 1A). Heterozygous *Spidr*$^{+/-}$ mice were mated and gave birth to *Spidr*$^{-/-}$ offspring. *Spidr*$^{-/-}$ mice were born according to Mendelian proportions and had normal body weight (Supplementary Figure S2A and B). Immunoblotting using total protein extracts from the testes of both wild type (WT) and *Spidr*$^{-/-}$ males confirmed that SPIDR was successfully disrupted (Figure 1B).

We found that the *Spidr*$^{-/-}$ mice phenotype is sexually dimorphic since male knockout mice were sterile but females displayed subfertility. 6-week-old *Spidr*$^{-/-}$ males had much smaller testes than those of WT mice (Figure 1C). Adult testis weights from *Spidr*$^{-/-}$ mice were 3- to 4-fold lighter than that in WT mice (Figure 1D). *Spidr*$^{-/-}$ male mice were completely infertility (Figure 1E). Histological analysis of *Spidr*$^{-/-}$ testes showed impaired spermatogenesis in which no post-meiotic round or elongating spermatids appeared in the seminiferous tubules (Figure 1F, upper panel). No spermatozoa were found in the cauda epididymis of *Spidr*$^{-/-}$ males (Figure 1F, lower panel). This phenotype was similar with SWS1 and SWSAP1 null mutants (17).

Spidr$^{-/-}$ females also showed fertility defects. The number of pups from the WT females increased incrementally as expected, while fertility tests in female *Spidr*$^{-/-}$ mice exhibited significantly lower fertility than WT mice, and became completely sterile after a 3-month period (Figure 1G). Morphological studies showed that ovaries of 2-month-old *Spidr*$^{-/-}$ mice contained fewer oocytes than WT mice ovaries. At around 4 months, the *Spidr*$^{-/-}$ mice ovaries exhibited a near-complete loss of developing oocytes. At 6 months, *Spidr*$^{-/-}$ mice ovaries displayed complete loss of normal morphology and were fibrotic (Figure 1H). Collectively, these results show that SPIDR is required for fertility in both males and females.

SPIDR is highly expressed in tissues and meiotic germ cells

A significant reduction of post-meiotic germ cells in testes from *Spidr*$^{-/-}$ mice resembled that of other early HR-defective mice, such as *Dmc1*, *Meilb2*, and *Brme1* knockout mice (25–27). In order to study the role of SPIDR in homologous recombination during meiosis, we first analyzed SPIDR expression and localization. SPIDR was expressed in various mouse tissues, with especially high expression in adult testis, where meiotic prophase I occur (Supplementary Figure S1A). We therefore focused on the function of SPIDR in testis to more closely examine its expression patterns during spermatogenesis. Immunoblotting of total protein extracts from WT testes at increasing ages revealed that the SPIDR protein level started to increase at postnatal day 14 (PD14) (Supplementary Figure S1B). PD14 is a developmental stage when a great number of spermatocytes enter zygotene stage (28) and this thus suggests that SPIDR has an important function in the zygotene stage. These findings were consistent with the analysis of average SPIDR protein abundance in isolated germ cells based on data from previous studies (Supplementary Figure S1C) (29). Further, qPCR analysis of isolated germ cells verified that *Spidr* was highly transcribed in the zygotene stages (Supplementary Figure S1D). Taken together, these results suggest that SPIDR may function in homologous recombination during spermatogenesis.

Spidr-deficient spermatocytes show pachytene arrest with defects of synapsis and DSB repair

Considering that SPIDR was highly expressed in zygotene spermatocytes, and knock out of *Spidr* resulted in mice infertility, we performed fluorescence-activated cell sorting in order to explore the exact defects during *Spidr*$^{-/-}$ spermatogenesis. We found that *Spidr*$^{-/-}$ mice lack spermatocytes beyond the pachytene stage (Supplementary Figure S2C). We next investigated whether SPIDR is required for homologous recombination in meiosis. We first examined chromosomes during meiosis prophase I by immunostaining of the synaptonemal complex central element (SYCP1) and axial/lateral element (SYCP3); these are components of the synaptonemal complex, a tripartite proteinaceous structure that forms between the homologs (30). No diplotene spermatocytes were detectable in *Spidr*$^{-/-}$ testes, indicating the pachytene stage arrest (Figure 2A). We further quantified the percentage of spermatocytes at different stages of meiosis prophase I in WT and *Spidr*$^{-/-}$ testes. We found that spermatocytes failed to proceed beyond the early-pachytene stage and only 4.8% of spermatocytes reached early-pachytene stage in *Spidr*$^{-/-}$ testes. This was in sharp contrast to that 23.08% of spermatocytes had reached the early-pachytene stage at PD42 in WT testes (Figure 2B).

Additionally, abnormal synapsis was observed in *Spidr*$^{-/-}$ zygotene spermatocytes (Supplementary Figure S4A). It is observed as different regions of one chromosome synapsed with multiple partners. This results in frequent synapsis between non-homologous chromosomes, which has been reported in several early HR-defective mice (26,27,31). In *Spidr*$^{-/-}$ spermatocytes, 49.7% of zygotene cells showed abnormal synapses of heterologous chromosomes (Supplementary Figure S4B). Possibly, these zygotene spermatocytes with severe abnormal synapses were unable to enter the pachytene stage, which is supported by the high proportion of zygotene spermatocytes in the *Spidr*$^{-/-}$ testes (Figure 2B).

The completion of synapsis at pachytene stage is always accompanied by the completion of DSB repair on autosomes. Considering the defects of synapsis in *Spidr*$^{-/-}$ testes, we speculated that DSB repair would be impaired as well. The strength of the γH2AX signal can represent the degree of DSB damage (32). It appears in the leptotene stage upon DSB formation (32), and disappears from autosomes till the pachytene stage, but remains concentrated in the XY body from pachytene to diplotene stage (33). We therefore evaluated meiotic DSB repair by immunostaining γH2AX in spermatocytes and found that γH2AX signals were comparable between WT and *Spidr*$^{-/-}$ spermatocytes at the leptotene stage, suggesting that DSB formation was unaffected in *Spidr*$^{-/-}$ spermatocytes. However, γH2AX signals were still maintained on autosomes at pachytene-like stage in *Spidr*$^{-/-}$ spermatocytes, while γH2AX signals were only concentrated in the XY body at pachytene stage in WT spermatocytes (Figure 2C) (Supplementary Figure S3A).

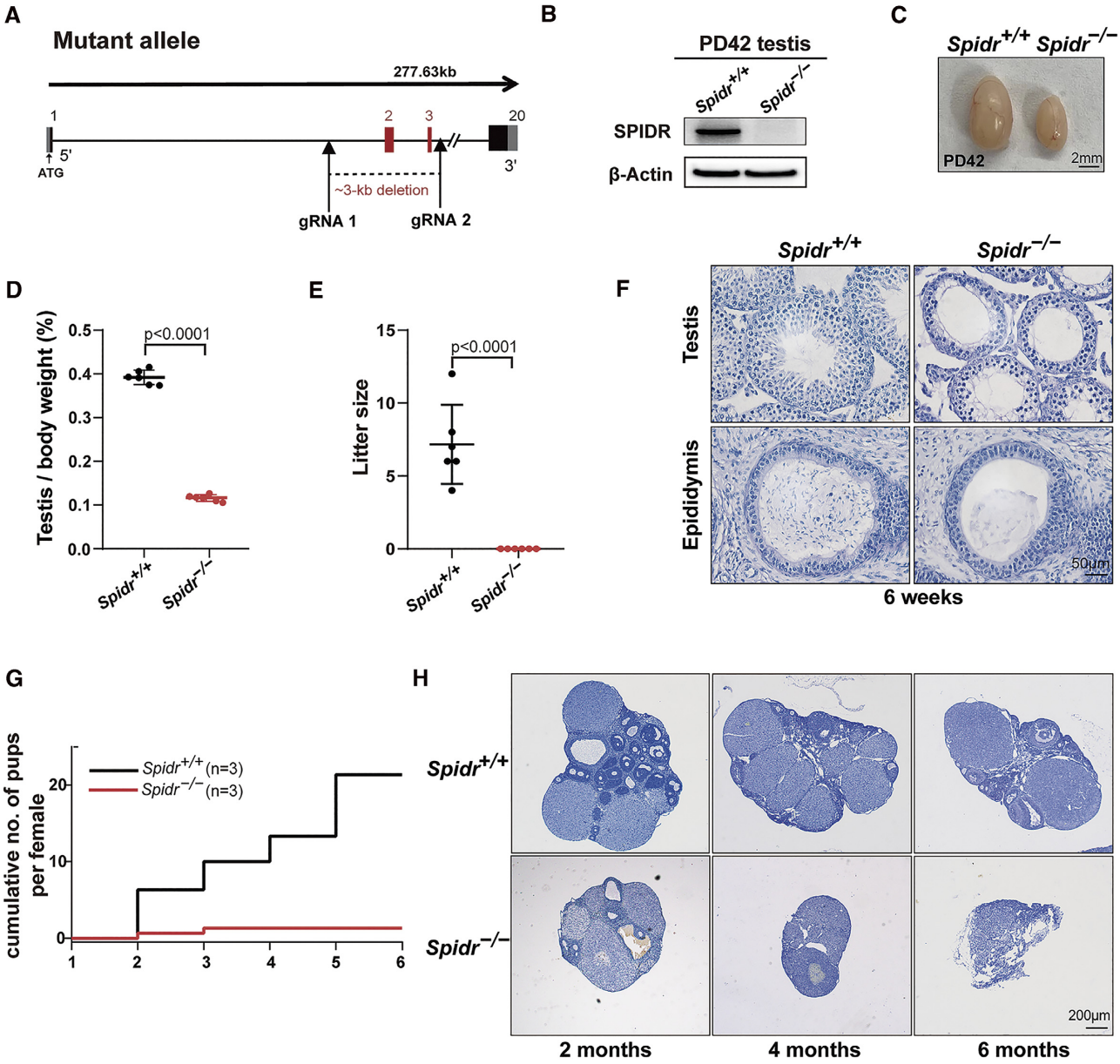

Figure 1. SPIDR is required for both male and female fertility. (**A**) Schematic representation of the CRISPR-Cas9 editing genome editing system to the *Spidr*-deficient mice. (**B**) Western blot of SPIDR in testes of WT and *Spidr*$^{-/-}$ mice at PD42. β-Actin was used as the loading control. PD, postnatal day. (**C**) Morphology of testes at PD42 in WT and *Spidr*$^{-/-}$ male mice. *Spidr*$^{-/-}$ testes were obviously smaller than WT at PD42. (**D**) Testis to body weight ratios of adult mice. *Spidr*$^{-/-}$ testes had significantly lower testis weight to body weight ratio compared to WT. Error bars, mean ± s.d. Student's *t*-test, two-tailed. (**E**) *Spidr*$^{-/-}$ male mice between 8–12 weeks were sterile with no offspring. $n = 3$ for each genotype. Error bar, mean ± s.d. (**F**) H&E staining of adult testis sections. The complete arrest of spermatogenesis in *Spidr*$^{-/-}$ mice is indicated by lack of spermatids or mature spermatozoa in the testis or epididymis. (**G**) Cumulative numbers of pups per female during the defined period. $n = 3$ mice per genotype. (**H**) Histological analysis of ovaries from WT and *Spidr*$^{-/-}$ females. Ovaries in 2-month-old *Spidr*$^{-/-}$ mice have fewer follicles than WT. At around 4 months of age, mutant ovaries exhibited a near-complete loss of developing follicles. At 6 months, *Spidr*$^{-/-}$ ovaries lose normal morphology.

Although it seems that chromosomes synapsed normally in *Spidr*$^{-/-}$ early pachytene stage spermatocytes, a considerable number of meiotic DSBs remained unrepaired in these *Spidr*$^{-/-}$ spermatocytes. Further, terminal deoxynucleotidyl transferase dUTP nick end labeling (TUNEL) assays revealed an increase in the number of apoptotic cells in the *Spidr*$^{-/-}$ testes compared to that of the WT (Supplementary Figure S2D). This indicates that the repair of DBS disruption could trigger the pachytene checkpoint, subsequently followed by the apoptosis of defective spermatocytes (34). SPIDR is therefore essential for the progression of meiotic recombination.

Crossover complexes and HR intermediates are defective in *spidr*-deficient spermatocytes

A small proportion of *Spidr*$^{-/-}$ spermatocytes still entered the pachytene stage, which led us to ask whether these

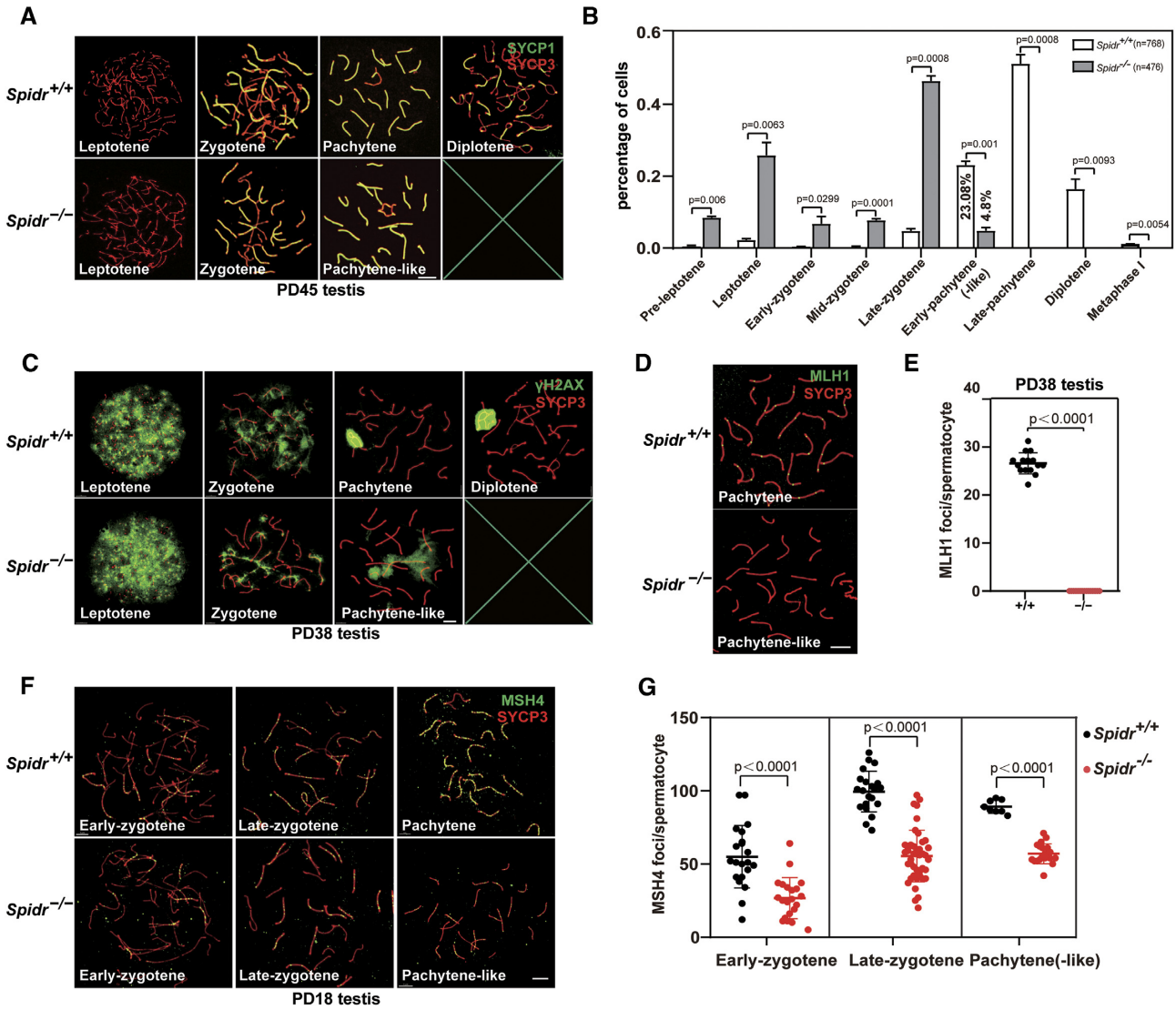

Figure 2. SPIDR is indispensable for meiotic progression. (**A**) Spermatocyte chromosome spreads from WT and *Spidr*$^{-/-}$ testes at PD45. Immunofluorescent signals for SYCP1 (green) and SYCP3 (red) indicate pachytene arrest in spermatocytes of *Spidr*$^{-/-}$ mice. Scale bars, 5 μm. (**B**) Proportions of WT and *Spidr*$^{-/-}$ spermatocytes in different meiotic stages, determined by calculating the number of spermatocytes at each stage divided by the total number of spermatocytes counted in adult testes. *P* values were calculated by Student's t-test. Error bars, mean ± s.d. (**C**) Representative images of spermatocyte chromosome spreads from WT and *Spidr*$^{-/-}$ testes at PD38 showing leptotene, zygotene, pachytene, and diplotene stages. Immunofluorescent signals for SYCP3 (red) and γH2AX (green) show that γH2AX persists around autosomes at pachytene in *Spidr*$^{-/-}$ spermatocytes, indicating incomplete DSB repair. Scale bars, 5 μm. (D, E) Representative images of WT and *Spidr*$^{-/-}$ spermatocytes immunostained for SYCP3 (red) and MLH1 crossover markers (green) (**D**) and quantification of foci for image (**E**). No MLH1 signal was detected in *Spidr*$^{-/-}$ spermatocytes compared to WT. Scale bars, 5μm. Error bars, mean ± s.d. (F, G) Representative images of WT and *Spidr*$^{-/-}$ spermatocytes immunostained for SYCP3 (red) and MSH4 (green) at the early-zygotene, late-zygotene, and pachytene stages are shown in (**F**). MSH4 foci counts were reduced in *Spidr*$^{-/-}$ spermatocytes. Quantification of foci for images in (**G**). *P* values were calculated by Student's *t*-test. Error bars, mean ± s.d. Scale bars, 5 μm.

spermatocytes can complete homologous recombination and form crossovers, which are marked by MLH1/HEII10 at middle to late pachytene stage (35–37). Approximately 20–30 MLH1/HEI10 foci per cell could be detected in WT pachytene spermatocytes, whereas no signal was observed in *Spidr*$^{-/-}$ pachytene spermatocytes (Figure 2D, E and Supplementary Figure S4C, D). Thus, crossover formation is completely defective in *Spidr*$^{-/-}$ spermatocytes.

It has been reported that the recombination factor MSH4 stabilizes DNA-strand exchange intermediates during homologous recombination, some of which will become crossovers mostly marked by MLH1 (11,38). We next immunostained MSH4 to investigate the effects of SPIDR deletion on the HR intermediates during meiosis prophase I. We detected reductions in the number of MSH4 foci in *Spidr*$^{-/-}$ spermatocytes compared to the WT from the early-zygotene stage to the pachytene stage: early-zygotene (26.667 ± 14.129 in *Spidr*$^{-/-}$ versus 54.952 ± 21.306 in WT), late-zygotene (55.442 ± 17.602 in *Spidr*$^{-/-}$ versus 99.476 ± 13.941 in WT), and pachytene (57 ± 6.751 in *Spidr*$^{-/-}$ versus 89.125 ± 4.390 in WT) (Figure 2F, G). Taken together, these results suggest that SPIDR is required

for HR intermediates stabilization and crossover formation during meiosis homologous recombination.

SPIDR is indispensable for the recruitment of recombinase RAD51 and DMC1

To support meiotic recombination and synapsis progression, recombinase RAD51 and its meiosis-specific paralog DMC1 are recruited and assembled to form ssDNA filaments that facilitate scanning for homologous pairing regions (6,39,40). RAD51 and DMC1 foci were counted to assess the effects of *Spidr*-deficient on early homologous recombination. We found that *Spidr*$^{-/-}$ spermatocytes exhibited a reduction in RAD51 foci at leptotene stage (28 ± 7.892 in *Spidr*$^{-/-}$ versus 150.6 ± 42.88 in WT), zygotene stage (67.82 ± 27.84 in *Spidr*$^{-/-}$ versus 184.7 ± 55.67 in WT), and pachytene stage (8.857 ± 6.388 in *Spidr*$^{-/-}$ versus 34.30 ± 11.04 in WT) (Figure 3A, B). Similarly, the number of DMC1 foci was also greatly reduced in *Spidr*$^{-/-}$ spermatocytes compared to WT at leptotene stage (67.1 ± 10.567 in *Spidr*$^{-/-}$ versus 121.1 ± 33.099 in WT), zygotene stage (82.846 ± 23.954 in *Spidr*$^{-/-}$ versus 163.538 ± 27.235 in WT), and pachytene stage (26.429 ± 10.143 in *Spidr*$^{-/-}$ versus 68.7 ± 13.174 in WT) with no significant change in the fluorescence intensity (Figure 3C, D and Supplementary Figure S3C, D). The reduction of RAD51 and DMC1 foci in *Spidr*$^{-/-}$ spermatocytes is also supported by a previous study (18).

Before the formation of ssDNA filaments, the long single strand 3' overhangs were coated by RPA complex, which subsequently were replaced by RAD51 and DMC1 (7). An increase in RPA foci at leptotene stage (290 ± 26.291 in *Spidr*$^{-/-}$ versus 217.375 ± 41.071 in WT), zygotene stage (284.1 ± 49.253 in *Spidr*$^{-/-}$ versus 257 ± 61.514 in WT), and pachytene stage (185 ± 9.472 in *Spidr*$^{-/-}$ versus 148.6 ± 17.422 in WT) were observed in *Spidr*$^{-/-}$ spermatocytes compared to WT (Supplementary Figure S4E, F), indicating accumulated end-resected intermediates. Further, the RPA foci exhibited brighter in *Spidr*$^{-/-}$ spermatocytes at zygotene stage (Supplementary Figure S3B). There is a possible explanation for this phenotypic difference. In *Spidr*$^{-/-}$ spermatocytes, the inefficient loading of RAD51 and DMC1 on ssDNA delayed the homology searching and strand exchange, and resulted in the RPA foci' s aberrant retention.

To determine whether SPIDR interacts with the homologous recombinase RAD51 and DMC1, we carried out co-immunoprecipitation (co-IP) in 293T cells, and found that both MYC-RAD51 and MYC-DMC1 were pulled-down by FLAG-SPIDR; noteworthy, this was not disrupted upon the addition of DNase, suggesting that the detected interaction is not dependent on DNA (Figure 3E). Further, a yeast-two-hybrid (Y2H) assays also supported the idea that SPIDR interacts with RAD51 and DMC1. SPIDR's N terminus (1–500aa) mediates the SPIDR-RAD51 interaction (Figure 3F, second panels), while the interaction of SPIDR-DMC1 is mediated by both SPIDR's N (1–500aa) and C termini (501–933aa) (Figure 3F, third panels).

A previous study found that BLM focus formation was severely impaired in SPIDR-depleted U2OS cells (12), which motivated us to examine whether BLM foci formation is impaired in *Spidr*$^{-/-}$ spermatocytes during meiotic recombination. Immunostaining against BLM showed no defects in *Spidr*$^{-/-}$ spermatocytes compared with WT, which is quite different from that observed in human somatic cells (Supplementary Figure S4G, H). Thus, SPIDR is required for the assembly of RAD51 and DMC1 foci, but not of BLM foci, during meiotic recombination.

Spidr$^{-/-}$ oocytes exhibit defects in meiotic recombination

Chromosome spreads from different stages of embryonic female *Spidr*$^{-/-}$ mice showed that meiosis initiates normally, and progress to pachytene stage at embryonic day17.5 (E17.5) (Figure 4A). However—and similar to our findings in males showing that few *Spidr*$^{-/-}$ spermatocytes proceeded to pachytene—we found that only 7.5% of *Spidr*$^{-/-}$ female oocytes reach pachytene stage at E17.5, whereas 58.8% of WT female oocytes reach pachytene stage (Figure 4B). These results clearly suggested that the meiotic progression was delayed in *Spidr*$^{-/-}$ female oocytes.

To investigate whether the SPIDR-dependent assembly of RAD51 and DMC1 is essential for meiosis progression in oocytes, immunostaining of RAD51 and DMC1 were implemented in E17.5 oocytes. *Spidr*$^{-/-}$ oocytes display reduction in RAD51 (75.67 ± 13.78 in *Spidr*$^{-/-}$ versus 107.1 ± 25.64 in WT) and DMC1 (106.3 ± 36.15 in *Spidr*$^{-/-}$ versus 150.1 ± 42.35 in WT) foci at zygotene stage (Figure 4C–F). The degree of RAD51 and DMC1 foci reduction is milder in oocytes as compared with that in spermatocytes.

Remarkably, MLH1 foci were detectable in *Spidr*$^{-/-}$ oocytes with a reduction at pachytene stage (16.00 ± 2.507 in *Spidr*$^{-/-}$ versus 22.09 ± 3.330 in WT) (Figure 4G, H), indicating that a small proportion of CO-defective oocytes entered the mid-pachytene stage. We further studied whether such CO-defective oocytes could develop into normal follicles after birth. The absence of chiasma causes the failure of univalent chromosomes to align properly while attaching to microtubules at the metaphase plate, which can trigger a spindle assembly checkpoint (SAC) and block anaphase progression (41,42). Only 5.8% of metaphase I (MI) oocytes showed univalent chromosomes (arrowhead) marked by Topoisomerase II (TOP2) which localized on chromosome arms in *Spidr*$^{-/-}$ oocytes, indicating that most CO-defective oocytes can escape SAC (Supplementary Figure S5C and D). However, in above 5.8% oocytes, abnormal bivalent formation of a few chromosome pairs is inefficient for triggering the SAC, allowing such oocytes to survive and thus predisposing to aneuploidy (43). Thus, we analyzed the percentage of aneuploid metaphase II oocytes and found that there was only 3.8% aneuploid oocytes in *Spidr*$^{-/-}$ mice (Supplementary Figure S5E and F). These findings suggest that most CO-defective oocytes can complete meiosis and develop backward into follicles to support the fertility of *Spidr*$^{-/-}$ females after birth; this is quite different from complete pachytene arrest in *Spidr*$^{-/-}$ males.

Knockout of *spidr* leads to POI

A homozygous nonsense mutation in the SPIDR was reported to be related to an autosomal recessive premature

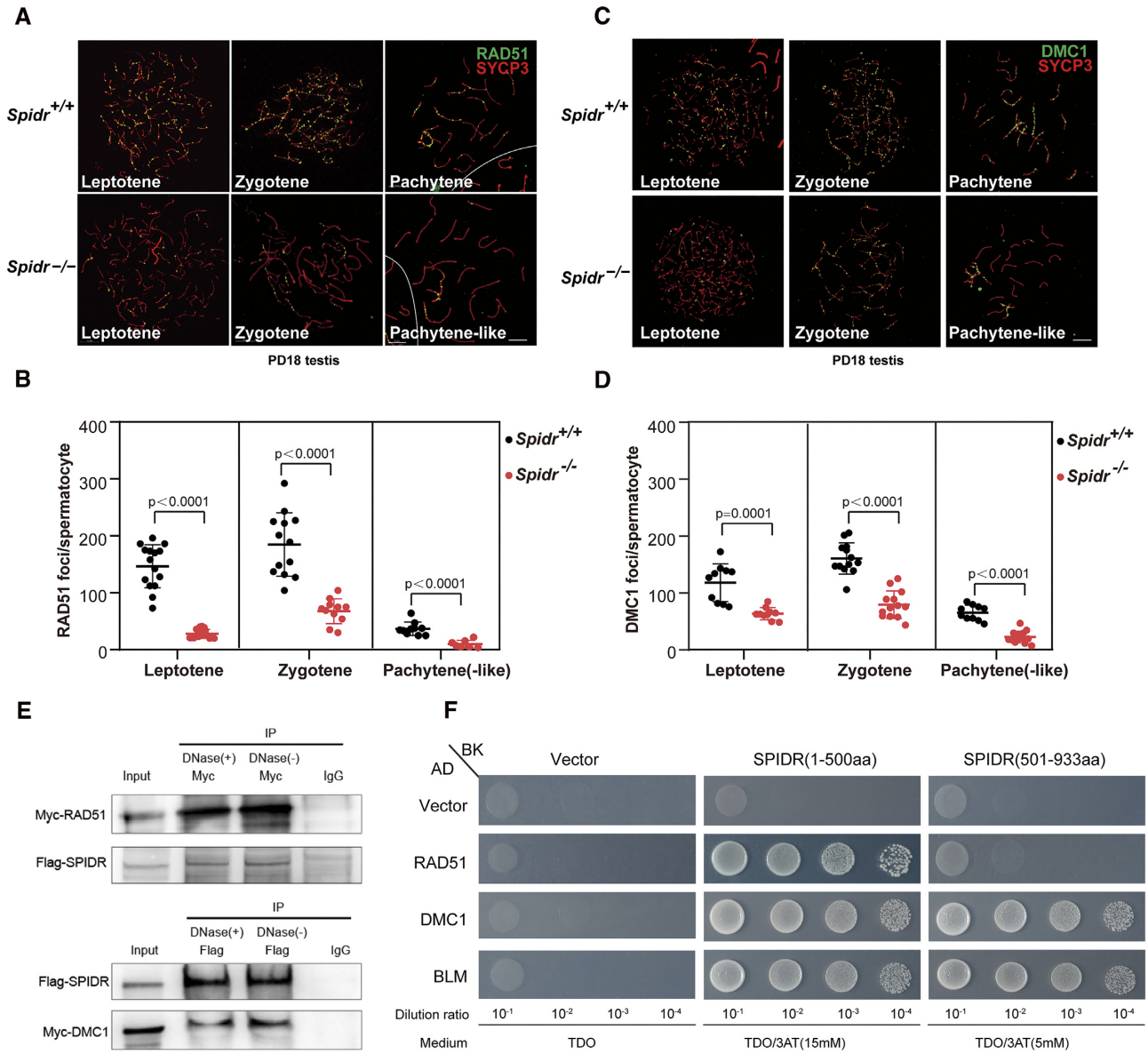

Figure 3. SPIDR is indispensable for the recruitment of recombinase RAD51 and DMC1. (A–D) Representative images of WT and *Spidr*$^{-/-}$ spermatocytes immunostained for SYCP3 (red) and DMC1/RAD51 (green) at the leptotene, zygotene, and pachytene stages are shown in (**A**, **C**). DMC1/RAD51 foci counts were reduced in *Spidr*$^{-/-}$ spermatocytes. Quantification of foci for images in (**B**, **D**). *P* values were calculated by Student's *t*-test. Error bars, mean ± s.d. Scale bars, 5 μm. (**E**) Co-Immunoprecipitation analysis of SPIDR and RAD51/DMC1 from 293T cells extracts which overexpressed these three proteins. (**F**) Yeast-two-hybrid: SPIDR(1–500aa) interacts with RAD51/DMC1/BLM in the second panels, while SPIDR (501–933aa) interacts with DMC1/BLM in the third panels with SPIDR as bait and RAD51/DMC1/BLM as prey. The degree of dilution of fungus solution increased from left to right.

ovarian insufficiency (POI) (44). POI, characterized by cessation of menstruation before menopause with elevated gonadotropin levels, is mostly caused by premature exhaustion of the PFP with multiple mechanisms (19,20). The PFP based on oocytes arresting at the diplotene stage of meiosis prophase I represents the ovarian reserve that determines fertility (20–22). To determine whether the loss of follicles within three months in *Spidr*$^{-/-}$ female mice was caused by the defective meiosis progression, ovaries dissected from E13.5 (embryonic day 13.5), E15.5 (embryonic day 15.5) and PD1 (postnatal day 1) mice were immunostained with mouse vasa homolog (MVH) antibody in which MVH marks for primordial germ cells (45). Quantification of relative numbers of oocytes showed that there were comparable numbers of oocytes in WT and *Spidr*$^{-/-}$ ovaries at E13.5 when meiosis is initiated (Figure 5A–C) and at E15.5 when the oocytes are just entering the pachytene stage (Figure 5D–F) (46). However, there was only 8.2% oocytes in *Spidr*$^{-/-}$ ovaries compared to WT ovaries at PD1 (Figure 5G–I). Thus, oocytes failing to proceed to pachytene stage were likely the reason for the exhaustion of PFP in *Spidr*$^{-/-}$ mice. Due to the depletion of PFP, the primary follicles decreased greatly on PD8 and PD15 in *Spidr*$^{-/-}$ ovaries (Supplementary Figure S5A), and that 3–5w *Spidr*$^{-/-}$ female

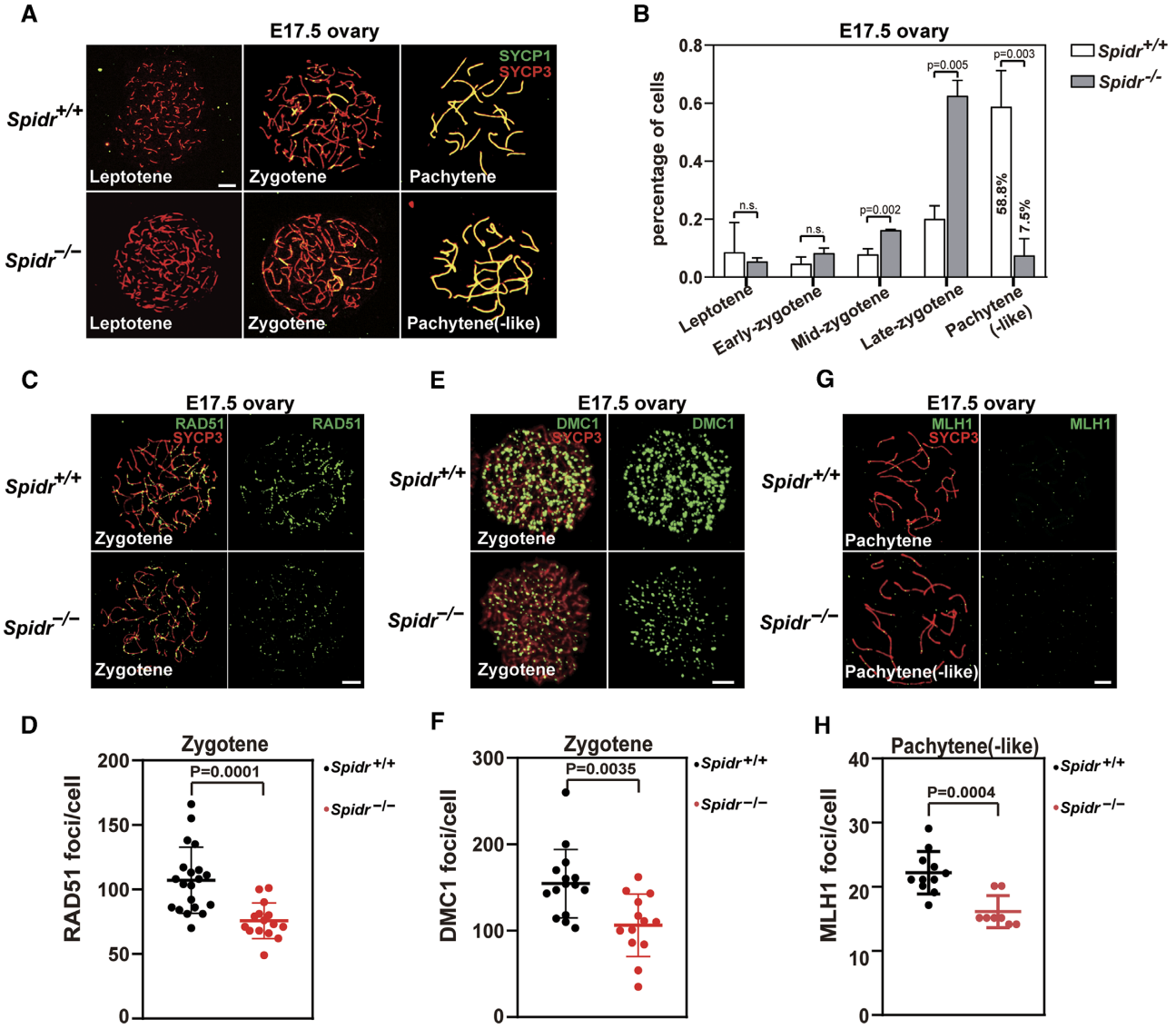

Figure 4. Defective meiotic progression in *Spidr*$^{-/-}$ oocytes. (**A**) Representative images of oocytes immunostained for SYCP3 (red) and SYCP1 (green) at the leptotene, zygotene, and pachytene in WT and *Spidr*$^{-/-}$ mice. Scale bars, 5 μm. Error bars, mean ± s.d. (**B**) Proportions of WT and *Spidr*$^{-/-}$ oocytes in different meiotic stages, determined by calculating the number of oocytes at each stage divided by the total number of oocytes counted in E17.5 ovaries. *P* values were calculated by Student's *t*-test. Error bars, mean ± s.d. (C–H) Representative images of WT and *Spidr*$^{-/-}$ oocytes immunostained for SYCP3 (red) and RAD51/DMC1/MLH1 (green) in E17.5 ovaries (**C**, **E**, **G**). RAD51/DMC1/MLH1 focus counts are reduced in *Spidr*$^{-/-}$ oocytes. Quantification of foci for images in (**D**, **F**, **H**). Scale bars, 5μm. P values were calculated by Student's *t*-test. Error bars, mean ± s.d.

mice showed apparently fewer follicles (Supplementary Figure S5B), which led to POI at 3–4 months (Figure 1H).

Considering that *Spidr*$^{-/-}$ oocytes also exhibit defects in meiotic recombination, we concluded that SPIDR is also required for recombinase RAD51 and DMC1 recruitment and/or stabilization during female meiotic recombination. However, the defects of *Spidr*$^{-/-}$oocytes meiotic recombination were milder than that in males, and consequently led to premature ovarian insufficiency in *Spidr*$^{-/-}$ female mice.

Spidr$^{-/-}$*chk2*$^{-/-}$ females but not males are fertile

It has been reported that oocyte loss in other Shu complex subunits, SWS1 and SWSAP1, could be completely rescued by eliminating the DNA damage checkpoint kinase CHK2 (17). By contrast, we observed that oocyte loss was only partially rescued in *Spidr*$^{-/-}$*Chk2*$^{-/-}$ adult mice (Figure 6A). Further, *Spidr*$^{-/-}$*Chk2*$^{-/-}$ females were able to produce more offsprings than *Spidr*$^{-/-}$ females within 6 months (Figure 6B). These results suggest that the rescue by CHK2 ablation is likely better in *Sws1* and *Swsap1* mutants than that observed in *Spidr*$^{-/-}$ mice, and CHK2 is indispensable for oocyte elimination in the Shu complex subunit mutants (17).

In contrast to females, *Spidr*$^{-/-}$*Chk2*$^{-/-}$ males exhibit only minimal rescue. There were no spermatozoa in the *Spidr*$^{-/-}$*Chk2*$^{-/-}$ epididymis (Supplementary Figure S6A). However, the meiosis process continued to move

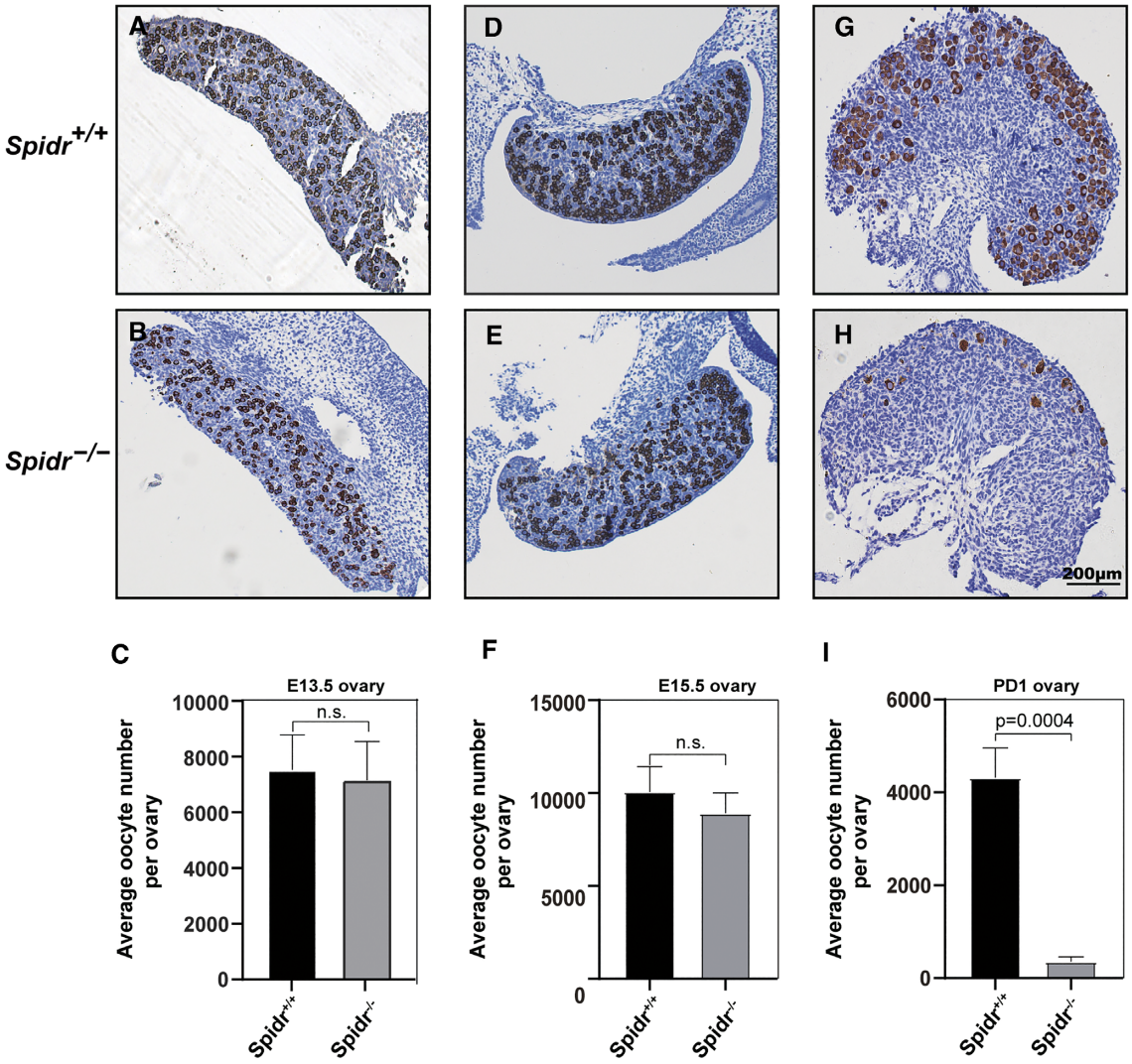

Figure 5. Knockout of *Spidr* leads to POI. (A, B) Representative WT (**A**) and *Spidr*$^{-/-}$ (**B**) ovary sections from E13.5 females immunostained for mouse vasa homolog (MVH) with hematoxylin counterstaining. (**C**) Average oocyte counts showed that there were similar numbers of oocytes in E13.5 WT and *Spidr*$^{-/-}$ females before entering into meiosis. (D, E) Representative WT (**D**) and *Spidr*$^{-/-}$ (**E**) ovary sections from E15.5 females immunostained for MVH with hematoxylin counterstaining. (**F**) Average oocyte counts showed that *Spidr*$^{-/-}$ ovaries contained insignificantly fewer oocytes than WT ovaries when just entering pachytene. (G, H) Representative WT (**G**) and *Spidr*$^{-/-}$ (**H**) ovary sections from PD1 females immunostained for MVH with hematoxylin counterstaining. (**I**) Average oocyte counts showed that *Spidr*$^{-/-}$ ovaries contained significantly fewer follicles than WT ovaries after birth. In all cases, MVH-positive cells were counted. Counts were made for every section (5 μm per section) and summed to calculate the total number of oocytes per ovary. For each genotype, three ovaries were analyzed. *P* values were calculated by Student's *t*-test. Error bars, mean ± s.d. Scale bars, 200 μm.

forward upon deletion of CHK2, which is demonstrated by the observations of diplotene and metaphase I cells in *Spidr*$^{-/-}$*Chk2*$^{-/-}$ testes (Figure 6C). Post-meiotic cells marked by MSY2 which is highly expressed in post meiotic round spermatids (47) were present in *Spidr*$^{-/-}$*Chk2*$^{-/-}$ testes but not *Spidr*$^{-/-}$ testes (Supplementary Figure S6B). These post-meiotic cells which escaped the checkpoint elimination even developed into round or elongating spermatids in *Spidr*$^{-/-}$*Chk2*$^{-/-}$ testes (Figure 6D). Thus, CHK2 is critical for oocyte and spermatocyte elimination in *Spidr*$^{-/-}$ mice, but the rescue by CHK2 ablation exhibits a sex-dependent manner between *Spidr*$^{-/-}$ male and female.

DISCUSSION

In this study, we identified a function of SPIDR in meiotic recombination. The reduction in the number of RAD51 and DMC1 foci in the *Spidr*$^{-/-}$ mice resulted in abnormal repair of DSBs and abnormal synapsis. SPIDR is a subunit of the SWS1-SWSAP1-SPIDR complex and exerts regulatory effects on recombinases during homologous recombination. It appears that during meiotic recombination the SWS1-SWSAP1-SPIDR complex regulates the recruitment and/or stability of RAD51/DMC1 (Figure 6E).

Proper homologous recombination requires efficient assembly and stabilization of DMC1/RAD51 on ssDNA. Many accessory HR factors have been reported to

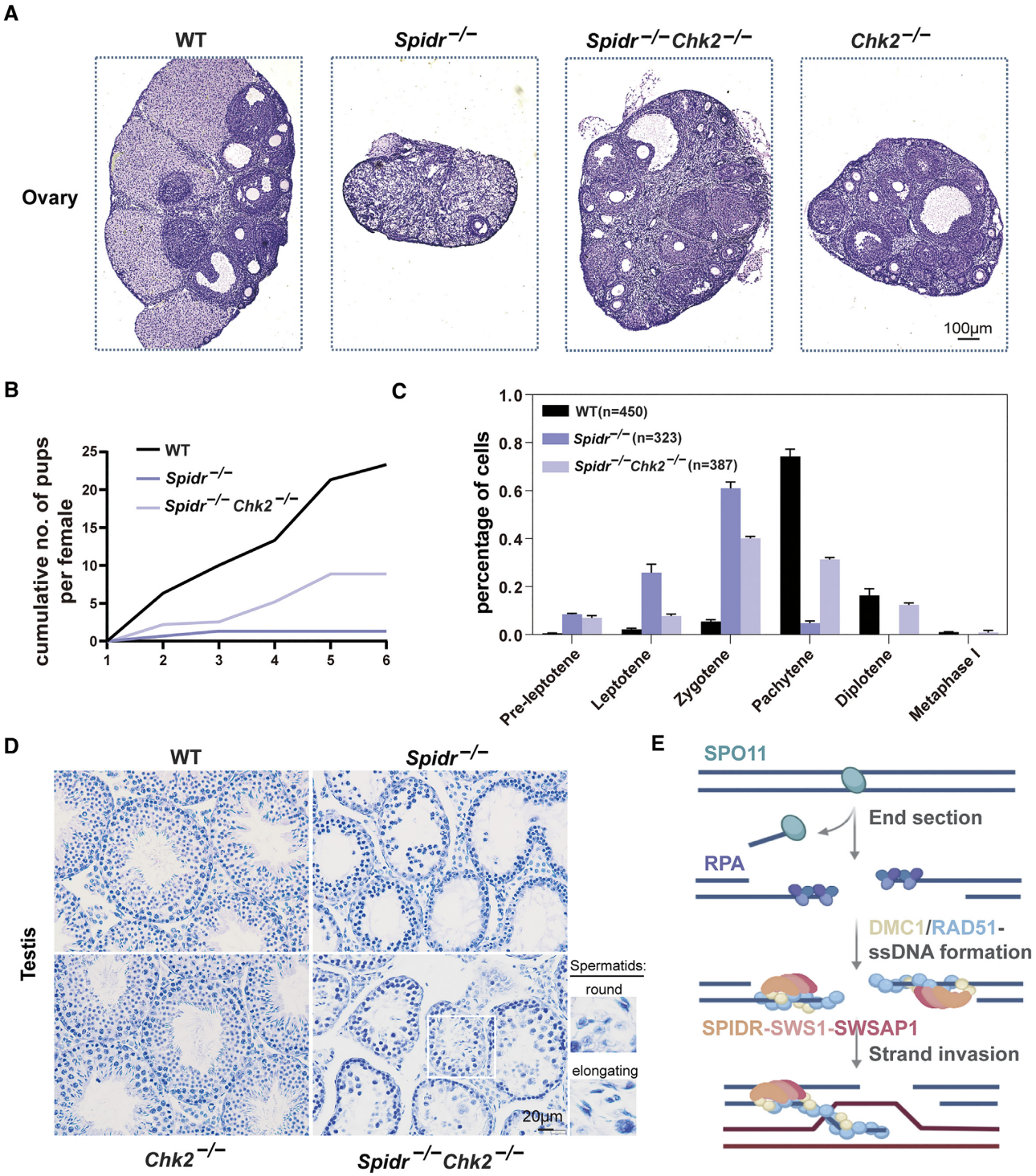

Figure 6. *Chk2* ablation rescues oogenesis and spermatogenesis of *Spidr*-deficient mice. (**A**) Histological analysis of ovaries showed that adult *Spidr*$^{-/-}$*Chk2*$^{-/-}$ ovaries have follicles at various stages of oocyte development, unlike *Spidr*$^{-/-}$ ovaries. (**B**) Cumulative numbers of pups per female within 6 months of age. $n = 3$ for each genotype. (**C**) Proportions of WT, *Spidr*$^{-/-}$ and *Spidr*$^{-/-}$*Chk2*$^{-/-}$ spermatocytes in different meiotic stages, determined by calculating the number of spermatocytes at each stage divided by the total number of spermatocytes counted in adult testes. (**D**) H&E staining of adult testis sections showed occasionally round and elongated spermatids in *Spidr*$^{-/-}$*Chk2*$^{-/-}$ tubules. (**E**) Proposed model for SPIDR function during meiotic recombination.

regulate this process (31,48–51). How these accessory HR factors promote or regulate DMC1/RAD51–ssDNA nucleoprotein filaments remain to be elucidated. In our study, *Spidr*-deficient mice have a reduction in RAD51 foci and DMC1 foci formation in the early step of meiosis which ultimately resulted in DSB repair defects. These defects are sufficient to render pachytene arrest while spermatocytes can progress to diplotene in *Brme1*-deficient and *Sws1-Swsap1*-deficient mice in which DSB defect also exist (17,25). These differences position SPIDR as an effective mediator protein for RAD51 and DMC1 nucleoprotein filament formation/stabilization, and DSB repair.

SPIDR specifically interacts with RAD51 and DMC1. In *Spidr*-deficient mice, RAD51/DMC1 foci are detected at a lower level compared with that of the WT mice. Even if it is not clear in mice, RAD51 has a supporting effect on DMC1 in catalytic meiotic recombination in budding yeast and arabidopsis (39,52). Thus, whether SPIDR directly supports DMC1 function or acts through RAD51 remains to be elucidated.

Although SPIDR is required for the formation of DMC1/RAD51 foci in both males and females, knockout of *spidr* yielded sex-dependent phenotypes: meiotic progression was fully arrested in $Spidr^{-/-}$ males, whereas some (albeit obviously reduced) COs were formed in $Spidr^{-/-}$ females, and this allowed oocytes to develop into primordial follicles that supported fertility in females up to 3 months. Several recombination accessory factors regulating DMC1/RAD51 are known to have sex-dependent impacts: HSF2BP and ATR only affect male meiosis and fertility but have no or little effects on female meiosis or fertility (51,53); this is in contrast to accessory factors that exert similar effects in both males and females (e.g. HOP2-MND1, MEIOB and the Shu complex SWS1-SWSAP1) (17,31,54). Since adult $Spidr^{-/-}$ males are sterile and females exhibit subfertility, its function depends on sex to some degree. This difference appears possible because the checkpoint is less stringent in females than that in males, thus meiotic errors could be tolerated in oogenesis but not in spermatogenesis (55,56).

We found that loss of the DNA damage checkpoint kinase CHK2 partially restores fertility to *Spidr*-deficient females but not males. This type of sex-specific, CHK2-mediated rescue has also been reported for *Swsap1* and *Trip3* knockout mice (17,57). Our study adds another layer of evidence supporting that CHK2 can be informatively conceptualized as a meiotic DNA damage checkpoint for the efficient elimination of abnormal oocytes but not spermatocytes, and this deeper understanding of DSB repair checkpoint should inform therapeutic developments towards treating POI.

In summary, our study provides a comprehensive analysis of meiotic phenotypes and function of SPIDR in homologous recombination. Moreover, distinct regulatory and sex-dependent phenotypes mediated by SPIDR allow us to uncover the association between function and biological environment.

DATA AVAILABILITY

No new data were generated or analysed in support of this research.

SUPPLEMENTARY DATA

Supplementary Data are available at NAR Online.

ACKNOWLEDGEMENTS

We thank R&D Team of SDU-CUHK for help with histological experiment. We also thank all our colleagues in the Chen laboratory for helpful discussions. We appreciate the support of the Translational Medicine Core Facility of Shandong University for consultation and instrument use.
Author contributions: H.B.L. and T.H. conceived and designed the entire project. X.W and T.H. performed most of the experiments. S.W. and Z.B. performed genotyping and RT-PCR. G.L., Z.-J.C. and H.B.L. supervised the whole project. X.W. and T.H. analyzed the data and wrote the manuscript with the assistance of the other authors. All authors read and approved the final manuscript.

FUNDING

National Key R&D Program of China [2022YFC2702600, 2018YFC1003400]; Research Unit of Gametogenesis and Health of ART-Offspring, Chinese Academy of Medical Sciences [2020RU001]; Academic Promotion Programme of Shandong First Medical University [2019U001]; Major Innovation Projects in Shandong Province [2021ZDSYS16]; Science Foundation for Distinguished Yong Scholars of Shandong [ZR2021JQ27]; Taishan Scholars Program for Young Experts of Shandong Province [tsqn202103192]; Basic Science Center Program of NSFC [31988101]; Shandong Provincial Key Research and Development Program [2020ZLYS02]. Funding for open access charge: National Key R&D Program of China [2022YFC2702600, 2018YFC1003400]; Research Unit of Gametogenesis and Health of ART-Offspring, Chinese Academy of Medical Sciences [2020RU001]; Academic Promotion Programme of Shandong First Medical University [2019U001]; Major Innovation Projects in Shandong Province [2021ZDSYS16]; Science Foundation for Distinguished Yong Scholars of Shandong [ZR2021JQ27]; Taishan Scholars Program for Young Experts of Shandong Province [tsqn202103192]; Basic Science Center Program of NSFC [31988101]; Shandong Provincial Key Research and Development Program [2020ZLYS02].
Conflict of interest statement. None declared.

REFERENCES

1. Handel,M.A. and Schimenti,J.C. (2010) Genetics of mammalian meiosis: regulation, dynamics and impact on fertility. *Nat. Rev. Genet.*, **11**, 124–136.
2. Zickler,D. and Kleckner,N. (2015) Recombination, pairing, and synapsis of homologs during meiosis. *Cold Spring Harb. Perspect. Biol.*, **7**, a016626.
3. Keeney,S., Giroux,C.N. and Kleckner,N. (1997) Meiosis-specific DNA double-strand breaks are catalyzed by Spo11, a member of a widely conserved protein family. *Cell*, **88**, 375–384.
4. Garcia,V., Phelps,S.E., Gray,S. and Neale,M.J. (2011) Bidirectional resection of DNA double-strand breaks by Mre11 and Exo1. *Nature*, **479**, 241–244.
5. Neale,M.J., Pan,J. and Keeney,S. (2005) Endonucleolytic processing of covalent protein-linked DNA double-strand breaks. *Nature*, **436**, 1053–1057.
6. Brown,M.S. and Bishop,D.K. (2014) DNA strand exchange and RecA homologs in meiosis. *Cold Spring Harb. Perspect. Biol.*, **7**, a016659.

7. Ribeiro,J., Abby,E., Livera,G. and Martini,E. (2016) RPA homologs and ssDNA processing during meiotic recombination. *Chromosoma*, **125**, 265–276.
8. Bachrati,C.Z., Borts,R.H. and Hickson,I.D. (2006) Mobile D-loops are a preferred substrate for the Bloom's syndrome helicase. *Nucleic Acids Res.*, **34**, 2269–2279.
9. Bzymek,M., Thayer,N.H., Oh,S.D., Kleckner,N. and Hunter,N. (2010) Double Holliday junctions are intermediates of DNA break repair. *Nature*, **464**, 937–941.
10. Gray,S. and Cohen,P.E. (2016) Control of meiotic crossovers: from double-strand break formation to designation. *Annu. Rev. Genet.*, **50**, 175–210.
11. Hunter,N. (2015) Meiotic recombination: the essence of heredity. *Cold Spring Harb. Perspect. Biol.*, **7**, a016618.
12. Wan,L., Han,J., Liu,T., Dong,S., Xie,F., Chen,H. and Huang,J. (2013) Scaffolding protein SPIDR/KIAA0146 connects the Bloom syndrome helicase with homologous recombination repair. *Proc. Natl. Acad. Sci. U.S.A.*, **110**, 10646–10651.
13. Yuan,J. and Chen,J. (2013) FIGNL1-containing protein complex is required for efficient homologous recombination repair. *Proc. Natl. Acad. Sci. U.S.A.*, **110**, 10640–10645.
14. Martino,J., Brunette,G.J., Barroso-Gonzalez,J., Moiseeva,T.N., Smith,C.M., Bakkenist,C.J., O'Sullivan,R.J. and Bernstein,K.A. (2019) The human Shu complex functions with PDS5B and SPIDR to promote homologous recombination. *Nucleic Acids Res.*, **47**, 10151–10165.
15. Liu,T., Wan,L., Wu,Y., Chen,J. and Huang,J. (2011) hSWS1.SWSAP1 is an evolutionarily conserved complex required for efficient homologous recombination repair. *J. Biol. Chem.*, **286**, 41758–41766.
16. Zhang,S., Wang,L., Tao,Y., Bai,T., Lu,R., Zhang,T., Chen,J. and Ding,J. (2017) Structural basis for the functional role of the Shu complex in homologous recombination. *Nucleic Acids Res.*, **45**, 13068–13079.
17. Abreu,C.M., Prakash,R., Romanienko,P.J., Roig,I., Keeney,S. and Jasin,M. (2018) Shu complex SWS1-SWSAP1 promotes early steps in mouse meiotic recombination. *Nat. Commun.*, **9**, 3961.
18. Prakash,R., Sandoval,T., Morati,F., Zagelbaum,J.A., Lim,P.X., White,T., Taylor,B., Wang,R., Desclos,E.C.B., Sullivan,M.R. *et al.* (2021) Distinct pathways of homologous recombination controlled by the SWS1-SWSAP1-SPIDR complex. *Nat. Commun.*, **12**, 4255.
19. De Vos,M., Devroey,P. and Fauser,B.C.J.M. (2010) Primary ovarian insufficiency. *Lancet North Am. Ed.*, **376**, 911–921.
20. Qin,Y., Jiao,X., Simpson,J.L. and Chen,Z.J. (2015) Genetics of primary ovarian insufficiency: new developments and opportunities. *Hum. Reprod. Update*, **21**, 787–808.
21. Llarena,N. and Hine,C. (2021) Reproductive longevity and aging: geroscience approaches to maintain long-term ovarian fitness. *J. Gerontol. A Biol. Sci. Med. Sci.*, **76**, 1551–1560.
22. Bolcun-Filas,E. and Handel,M.A. (2018) Meiosis: the chromosomal foundation of reproduction. *Biol. Reprod.*, **99**, 112–126.
23. Sun,Y.C., Sun,X.F., Dyce,P.W., Shen,W. and Chen,H. (2017) The role of germ cell loss during primordial follicle assembly: a review of current advances. *Int. J. Biol. Sci.*, **13**, 449–457.
24. Li,M., Huang,T., Li,M.J., Zhang,C.X., Yu,X.C., Yin,Y.Y., Liu,C., Wang,X., Feng,H.W., Zhang,T. *et al.* (2019) The histone modification reader ZCWPW1 is required for meiosis prophase I in male but not in female mice. *Sci. Adv.*, **5**, eaax1101.
25. Zhang,J., Gurusaran,M., Fujiwara,Y., Zhang,K., Echbarthi,M., Vorontsov,E., Guo,R., Pendlebury,D.F., Alam,I., Livera,G. *et al.* (2020) The BRCA2-MEILB2-BRME1 complex governs meiotic recombination and impairs the mitotic BRCA2-RAD51 function in cancer cells. *Nat. Commun.*, **11**, 2055.
26. Pittman,D.L., Cobb,J., Schimenti,K.J., Wilson,L.A., Cooper,D.M., Brignull,E., Handel,M.A. and Schimenti,J.C. (1998) Meiotic prophase arrest with failure of chromosome synapsis in mice deficient for Dmc1, a germline-specific RecA homolog. *Mol. Cell*, **1**, 697–705.
27. Zhang,J., Fujiwara,Y., Yamamoto,S. and Shibuya,H. (2019) A meiosis-specific BRCA2 binding protein recruits recombinases to DNA double-strand breaks to ensure homologous recombination. *Nat. Commun.*, **10**, 722.
28. Feng,C.W., Bowles,J. and Koopman,P. (2014) Control of mammalian germ cell entry into meiosis. *Mol. Cell. Endocrinol.*, **382**, 488–497.
29. Fang,K., Li,Q., Wei,Y., Zhou,C., Guo,W., Shen,J., Wu,R., Ying,W., Yu,L., Zi,J. *et al.* (2021) Prediction and validation of mouse meiosis-essential genes based on spermatogenesis proteome dynamics. *Mol. Cell. Proteomics*, **20**, 100014.
30. Schucker,K., Holm,T., Franke,C., Sauer,M. and Benavente,R. (2015) Elucidation of synaptonemal complex organization by super-resolution imaging with isotropic resolution. *Proc. Natl. Acad. Sci. U.S.A.*, **112**, 2029–2033.
31. Luo,M., Yang,F., Leu,N.A., Landaiche,J., Handel,M.A., Benavente,R., La Salle,S. and Wang,P.J. (2013) MEIOB exhibits single-stranded DNA-binding and exonuclease activities and is essential for meiotic recombination. *Nat. Commun.*, **4**, 2788.
32. Mahadevaiah,S.K., Turner,J.M., Baudat,F., Rogakou,E.P., de Boer,P., Blanco-Rodríguez,J., Jasin,M., Keeney,S., Bonner,W.M. and Burgoyne,P.S. (2001) Recombinational DNA double-strand breaks in mice precede synapsis. *Nat. Genet.*, **27**, 271–276.
33. Lam,I. and Keeney,S. (2014) Mechanism and regulation of meiotic recombination initiation. *Cold Spring Harb. Perspect. Biol.*, **7**, a016634.
34. Pacheco,S., Marcet-Ortega,M., Lange,J., Jasin,M., Keeney,S. and Roig,I. (2015) The ATM signaling cascade promotes recombination-dependent pachytene arrest in mouse spermatocytes. *PLoS Genet.*, **11**, e1005017.
35. Baker,S.M., Plug,A.W., Prolla,T.A., Bronner,C.E., Harris,A.C., Yao,X., Christie,D.M., Monell,C., Arnheim,N., Bradley,A. *et al.* (1996) Involvement of mouse Mlh1 in DNA mismatch repair and meiotic crossing over. *Nat. Genet.*, **13**, 336–342.
36. Marcon,E. and Moens,P. (2003) MLH1p and MLH3p localize to precociously induced chiasmata of okadaic-acid-treated mouse spermatocytes. *Genetics*, **165**, 2283–2287.
37. Anderson,L.K., Reeves,A., Webb,L.M. and Ashley,T. (1999) Distribution of crossing over on mouse synaptonemal complexes using immunofluorescent localization of MLH1 protein. *Genetics*, **151**, 1569–1579.
38. Storlazzi,A., Gargano,S., Ruprich-Robert,G., Falque,M., David,M., Kleckner,N. and Zickler,D. (2010) Recombination proteins mediate meiotic spatial chromosome organization and pairing. *Cell*, **141**, 94–106.
39. Cloud,V., Chan,Y.L., Grubb,J., Budke,B. and Bishop,D.K. (2012) Rad51 is an accessory factor for Dmc1-mediated joint molecule formation during meiosis. *Science*, **337**, 1222–1225.
40. Lao,J.P., Cloud,V., Huang,C.C., Grubb,J., Thacker,D., Lee,C.Y., Dresser,M.E., Hunter,N. and Bishop,D.K. (2013) Meiotic crossover control by concerted action of Rad51-Dmc1 in homolog template bias and robust homeostatic regulation. *PLoS Genet.*, **9**, e1003978.
41. Tachibana-Konwalski,K., Godwin,J., Borsos,M., Rattani,A., Adams,D.J. and Nasmyth,K. (2013) Spindle assembly checkpoint of oocytes depends on a kinetochore structure determined by cohesin in meiosis I. *Curr. Biol.*, **23**, 2534–2539.
42. Woods,L.M., Hodges,C.A., Baart,E., Baker,S.M., Liskay,M. and Hunt,P.A. (1999) Chromosomal influence on meiotic spindle assembly: abnormal meiosis I in female Mlh1 mutant mice. *J. Cell Biol.*, **145**, 1395–1406.
43. Singh,P., Fragoza,R., Blengini,C.S., Tran,T.N., Pannafino,G., Al-Sweel,N., Schimenti,K.J., Schindler,K., Alani,E.A., Yu,H. *et al.* (2021) Human MLH1/3 variants causing aneuploidy, pregnancy loss, and premature reproductive aging. *Nat. Commun.*, **12**, 5005.
44. Smirin-Yosef,P., Zuckerman-Levin,N., Tzur,S., Granot,Y., Cohen,L., Sachsenweger,J., Borck,G., Lagovsky,I., Salmon-Divon,M., Wiesmuller,L. *et al.* (2017) A Biallelic Mutation in the Homologous Recombination Repair Gene SPIDR Is Associated With Human Gonadal Dysgenesis. *J. Clin. Endocrinol. Metab.*, **102**, 681–688.
45. Fujiwara,Y., Komiya,T., Kawabata,H., Sato,M., Fujimoto,H., Furusawa,M. and Noce,T. (1994) Isolation of a DEAD-family protein gene that encodes a murine homolog of Drosophila vasa and its specific expression in germ cell lineage. *Proc. Natl. Acad. Sci. U.S.A.*, **91**, 12258–12262.
46. Wang,X. and Pepling,M.E. (2021) Regulation of meiotic prophase one in mammalian oocytes. *Front. Cell Dev. Biol.*, **9**, 667306.
47. Gu,W., Tekur,S., Reinbold,R., Eppig,J.J., Choi,Y.C., Zheng,J.Z., Murray,M.T. and Hecht,N.B. (1998) Mammalian male and female germ cells express a germ cell-specific Y-Box protein, MSY2. *Biol. Reprod.*, **59**, 1266–1274.
48. Yang,F., Eckardt,S., Leu,N.A., McLaughlin,K.J. and Wang,P.J. (2008) Mouse TEX15 is essential for DNA double-strand break

repair and chromosomal synapsis during male meiosis. *J. Cell Biol.*, **180**, 673–679.
49. Sharan,S.K., Pyle,A., Coppola,V., Babus,J., Swaminathan,S., Benedict,J., Swing,D., Martin,B.K., Tessarollo,L., Evans,J.P. *et al.* (2004) BRCA2 deficiency in mice leads to meiotic impairment and infertility. *Development*, **131**, 131–142.
50. Xu,X., Aprelikova,O., Moens,P., Deng,C.X. and Furth,P.A. (2003) Impaired meiotic DNA-damage repair and lack of crossing-over during spermatogenesis in BRCA1 full-length isoform deficient mice. *Development*, **130**, 2001–2012.
51. Widger,A., Mahadevaiah,S.K., Lange,J., ElInati,E., Zohren,J., Hirota,T., Pacheco,S., Maldonado-Linares,A., Stanzione,M., Ojarikre,O. *et al.* (2018) ATR is a multifunctional regulator of male mouse meiosis. *Nat. Commun.*, **9**, 2621.
52. Da Ines,O., Degroote,F., Goubely,C., Amiard,S., Gallego,M.E. and White,C.I. (2013) Meiotic recombination in Arabidopsis is catalysed by DMC1, with RAD51 playing a supporting role. *PLoS Genet.*, **9**, e1003787.
53. Brandsma,I., Sato,K., van Rossum-Fikkert,S.E., van Vliet,N., Sleddens,E., Reuter,M., Odijk,H., van den Tempel,N., Dekkers,D.H.W., Bezstarosti,K. *et al.* (2019) HSF2BP interacts with a conserved domain of BRCA2 and is required for mouse spermatogenesis. *Cell Rep.*, **27**, 3790–3798.
54. Pezza,R.J., Voloshin,O.N., Volodin,A.A., Boateng,K.A., Bellani,M.A., Mazin,A.V. and Camerini-Otero,R.D. (2014) The dual role of HOP2 in mammalian meiotic homologous recombination. *Nucleic Acids Res.*, **42**, 2346–2357.
55. Hunt,P.A. and Hassold,T.J. (2002) Sex matters in meiosis. *Science*, **296**, 2181–2183.
56. Morelli,M.A. and Cohen,P.E. (2005) Not all germ cells are created equal: aspects of sexual dimorphism in mammalian meiosis. *Reproduction*, **130**, 761–781.
57. Bolcun-Filas,E., Rinaldi,V.D., White,M.E. and Schimenti,J.C. (2014) Reversal of female infertility by Chk2 ablation reveals the oocyte DNA damage checkpoint pathway. *Science*, **343**, 533–536.